Moncho Esteve, IJ.; Gasque Albalate, M.; González Altozano, P.; Palau-Salvador, G. (2017). Simple inlet devices and their influence on thermal stratification in a hot water storage tank. Energy and Buildings. 150:625-638. doi:10.1016/j.enbuild.2017.06.012

Simple inlet devices and their influence on thermal stratification in a hot water storage tank.

Ignacio José Moncho-Esteve[1] (*Corresponding author*), María Gasque[2], Pablo González-Altozano[1], Guillermo Palau-Salvador[1].

Universitat Politècnica de València. Camino de Vera s/n. 46022 Valencia (Spain)

e-mail: igmones@doctor.upv.es

Tlf.: 0034-629936415

Fax: 0034-963877549

[1] Dpt. Ingeniería Rural y Agroalimentaria

[2] Dpt. Física Aplicada.

HIGHLIGHTS:

- Stratification and hydrodynamics of a hot water tank during charging are studied.
- A 3D-CFD model was used to supplement previous experimental analyses.
- A high degree of correlation with experiments and versatility was achieved.
- New inlet configurations and two inflow rates were simulated and compared.
- The role of some inlet characteristics on stratification is clarified.

ABSTRACT

Thermal energy storage is a technology used mostly in buildings and industries in order to preserve thermal energy so that the stored energy can be used at a later time. Thermal stratification during the charge process in a cylindrical water tank was investigated using tools of Computational Fluid Dynamics (CFD). Simulations were validated by means of experimental measurements of time-dependent temperature profiles. The results showed that the model was able to adequately capture the experimental temperature evolution in the tank for all the validation cases. Once validated the model, simple modifications of the usual inlet devices and inflow rate by CFD techniques were accomplished with the intention of improving the tank performance. It was found that the modifications of the simulated inlet devices affected the stratification level. This could lead to improve designs and optimize system efficiency. The analyses confirmed numerically the results obtained experimentally, and it was evidenced that a sintered bronze conical diffuser can improve stratification compared to a conventional bronze elbow inlet. Therefore, CFD techniques proved to be quite a valuable complement of experimental studies. The use of low inflow, smooth out inlet velocity and operate inflow upwards near the top of the tank enhanced stratification.

Keywords: Hot Water Storage Tank; Water Stratification; Inlet Parameters; Thermal Charging Efficiency; Unsteady Reynolds-Average Navier-Stokes (URANS).

Abbreviations

a	= face area vector
A (m^2)	= cell area
c ($J\ K^{-1}\ kg^{-1}$)	= specific heat capacity
c_{fg} ($J\ K^{-1}\ kg^{-1}$)	= specific heat capacity for fibreglass
c_{st} ($J\ K^{-1}\ kg^{-1}$)	= specific heat capacity for steel
CFD	= computational fluid dynamics
D	= sintered bronze conical diffuser
E (J)	= total energy
E	= elbow
f_g (N)	= body force vector
GCI	= grid convergence index
H (J)	= total enthalpy
H	= high case
I	= identity matrix
L	= low case
LES	= Large Eddy Simulation
M ($m^4\ s^{-2}$)	= jet momentum flux
MSE (K^2)	= mean squared error
n	= nº of experimental observations in a specific point along time
p (Pa)	= pressure
q''	= heat flux vector
Q_{in} ($L\ min^{-1}$)	= inflow
RE (-)	= relative error
RMSE (K)	= root mean squared error
t (min)	= time
t^* (-)	= dimensionless time
t_r (min)	= residence time
t_{ct} (min)	= charge time
T (K)	= temperature
T_{avg} (K)	= average temperature in the water domain
T_{amb} (K)	= ambient temperature
T_i (K)	= computed value of T at each ith experimental time step
$\hat{T}_i$ (K)	= experimental value of T at each ith experimental time step
T_{in} (K)	= inlet temperature
T_o (K)	= initial water tank temperature
TC	= thermocouple in the central zone
TES	= thermal energy storage
TL	= thermocouple in the lateral zone
U ($m\ s^{-1}$)	= velocity vector module
$\overline{U}$ ($m\ s^{-1}$)	= volume-weighted average velocity magnitude
U_{jet} ($m\ s^{-1}$)	= area-weighted average velocity on the nozzle section
U_n ($m\ s^{-1}$)	= normal velocity in the nozzle tip of the elbow
U_t ($m\ s^{-1}$)	= tangential velocity in the nozzle tip of the elbow
URANS	= unsteady Reynolds-average Navier-Stokes
v ($m\ s^{-1}$)	= velocity component
V (m^3)	= volume cell of each grid point
V_t (L)	= tank volume
y^+ (-)	= non-dimensional wall distance
η (-)	= thermal charging efficiency
θ (-)	= dimensionless temperature
λ ($W\ m^{-1}\ K^{-1}$)	= thermal conductivity
λ_{fg} ($W\ m^{-1}\ K^{-1}$)	= thermal conductivity for fibreglass
λ_{st} ($W\ m^{-1}\ K^{-1}$)	= thermal conductivity for steel
μ (Pa s)	=dynamic viscosity
ρ ($kg\ m^{-3}$)	= density
ρ_{fg} ($kg\ m^{-3}$)	= density for fibreglass
ρ_{st} ($kg\ m^{-3}$)	= density for steel
[T]	= viscous stress tensor

1 Introduction and objectives

Thermal energy systems are commonly suited to compensate heating loads. They require thermal energy storages (TES) to maintain the heated fluid when there is a mismatch between energy production and demand. A variety of solutions can be proposed at buildings, multiuser building, district, town or regional scale depending on the energy supply and demand patterns. Some of the most relevant aspects of thermal storage are treated in [1], [2] and [3]. In these systems, water is often used as the heat transfer fluid and storage in a tank given that is the cheapest option in sensible heat storages. Such tanks play an important role in promoting the efficiency of the energy system [4]. Thus, in system designs it is of paramount importance to pay attention to the thermal performance of the storage [5] wherein thermal stratification naturally takes place. Moreover, thermally stratified storage saves space and material [6], which is convenient for facility and building design.

Several public policies include renewable energy technologies [7] and certain laws claim to reduce progressively the energy consumption of buildings. Moreover, the stable thermal stratification is one of the most important aspects related to the efficiency of the thermal storage and therefore the system as a whole [8, 9] in a typically variable consumption behaviour of a household context.

The charging or discharging process of the storage significantly affects stratification. In the case of charging process, the level of mixing mostly depends on the inflow jet characteristics (*e.g.*, the momentum of the jet flow, direction and position) and the water inlet temperature. In particular, turbulence generated by the inlet devices may be one of the relevant mechanisms producing mixing. Therefore, an optimal design of these devices to uniformly circulate the flow into the tank can reduce mixing [10]–[12], thereby enhances the available energy of water. The effect of direct inlets on the stratification process during charging has been presented in many studies [11]–[19]. Moreover, mixing can also be induced by diffusion between the cold and the hot water, as well as heat conduction through the tank walls and loss of energy into the surroundings.

For the purpose of improving thermal performance, numerous methods and parameters are proposed in the literature to characterize the level of stratification or efficiency during charging, discharging and the stand-by period [20–22]. In many of them, the characterisation of the transient temperature profile in the tank is required [23], [24]. In this regard, the thermocline gradient and the thickness of the thermocline region have been employed in various works to evaluate the level of stratification [15], [25]–[27].

On the other hand, numerical models have been implemented to study thermal performance in water tanks in [5], [28], [29]. Moreover, experimental data from solar storage tanks were compared with different

numerical solutions in [30], [31]. In this context, 1D models are not able to adequately characterize flow structure [1] and current numerical studies are mainly two-dimensional [32]–[35]. Otherwise 3D approaches can provide more accurate and realistic results [36]–[38]. Thus, the use of 3D Computational Fluid Dynamics (CFD) approaches in recent researches can contribute towards supplementing and better understanding the physical phenomenon of stratification [39] as well as improving stratification and optimising designs [40]. Other researches [41] carried out 3D-CFD simulations for virtual prototyping and studied the influence of flow rate during discharging. A rigid stratifier was studied in [42] both with CFD and experimental procedures in a solar storage tank, for different inflow rates. CFD simulations and laboratory measurements of direct horizontal inlets at midheight of a solar combi-storage of about 800 L volume were presented in [43]; in this research, different inlet diffuser designs and recommendations were developed for different inlet mass flow rates.

Predicting the storage thermal performance solely by means of laboratory procedures can be difficult and expensive [5]. CFD modelling is then a very strong and useful tool to analyse 3D flows, even if turbulence caused by inlets is significant. Indeed, the high spatial and temporal resolution achieved with CFD methods may provide a more realistic characterization of thermal stratification when temperature-dependent indices are applied.

Experiments were carried out by [44] to investigate a rectangular storage tank with different inlet structures. The authors proposed the optimization of inlet to improve the performance of discharging. Moreover, within the framework of the present research, the stratification process was studied experimentally during thermal charging [45] by comparing the effect of different inflows through two inlet devices (a conventional elbow and a sintered bronze conical diffuser). It was concluded that a higher thermal stratification was achieved using the inlet diffuser, regardless of the flow tested. However, such a study provided only transient temperature data in the thermocouple locations for the experimental trials tested. In addition, the Virtual TC method was proposed by [46] to define the transient temperature profile avoiding the disadvantages related to the availability of discrete temperature data to calculate temperature-dependent indices in thermal stratification. However, hydrodynamics and their relation to stratification could not be examined in such experiments.

This work focuses on the study of flow field and thermal stratification during charging in a heat storage tank using water as the working fluid by means of CFD. It was intended that they will supplement the experimental analysis carried out in [45] and provide more precise information of the hydrodynamics and water stratification process. Thus, a robust and versatile CFD model was implemented with the purpose of

studying transient stratification in great detail, to better understand the role of some inlet geometrical characteristics and inflows in the magnitude and development of this process. The results of 3D Unsteady Reynolds-Averaged Navier-Stokes (URANS) simulations were validated with four experimental trials. Thereafter, simple inlet devices were proposed and their performances were analysed. These proposals were based in little modifications of the original inlets, which implied easy-to-implement and low-cost inlet modifications. Thus, the results of the simulations of the flow and heat transfer of six additional cases, based on different inlet configurations and inflow rates, are presented and analysed in this paper. The tank is a medium-sized cylindrical one, integrated in a direct (open loop) thermal energy system. The simulations were then analysed with the aim of proposing the keys that allow a better design of the inlets in the tank.

2 Materials and Methodology

2.1 Experimental setup

The experimental trials were conducted with a cylindrical hot water storage tank of 905 L capacity (800 mm inner diameter and 1800 mm height) made of steel, with a side and top wall thickness of 1.9 mm and 17 mm respectively. The side-walls, top and bottom were covered with a 50-mm-thick layer of insulating material (fibreglass). Two different inlet devices were fixed for the inflow: a bronze elbow (E1) and a sintered bronze conical diffuser (D1) which were arranged at the top of the tank, symmetrically with regard to the vertical axis. The experimental facility is described in more detail in [45]. A schematic diagram of experimental setup is showed in Figure 1.

In order to record the water temperature in the tank, two sets of 12 type T (Class 1) thermocouples were distributed uniformly and symmetrically along the vertical axis of the tank (150 mm apart and 75 mm from both the top and the bottom of the tank). One set were fixed in the central zone (TC) and the other on one side (TL) of the tank.

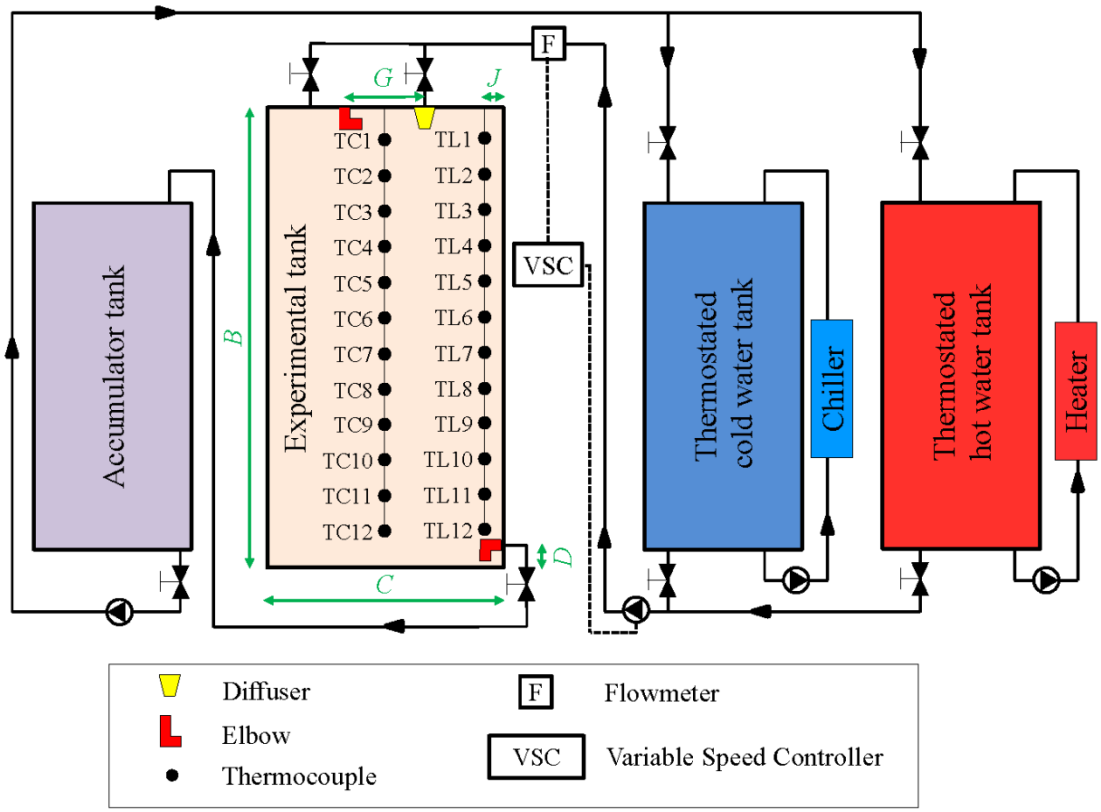

Fig. 1. Experimental setup. B = 1800 mm; C = 800 mm; D = 50 mm; G = 140 mm; J = 42 mm. TC: thermocouple in the central tank zone; TL: thermocouple in the lateral tank zone.

For validating the simulations, four thermal charging tests (Table 1) were carried out with the two inlet devices, elbow and diffuser, at two different flow rates. According to the regulations applied in thermal solar installations, the flow rate in a plant with a tank capacity similar to that used in this work (905 L), usually varies between 6-12 L·min^{-1}. Therefore, it was decided to use, on the one hand, a flow rate within the usual range relative to the capacity of the tank, but considered among the lowest values (6 L·min^{-1}, Low: L). On the other hand and with the aim of emphasizing the potential differences, a higher flow rate was used, out of that range, which was considered as a high flow rate (16 L·min^{-1}, High: H). The ambient temperature T_{amb} of the surroundings was also recorded and considered constant during each trial. The water tank temperature at the start of each trial T_o was 293±0.2 K. In all cases, a constant flow rate Q_{in} (L min^{-1}) was injected at 325.7±0.2 K until 120% of the total storage tank volume was replaced. This inlet temperature T_{in} is within the usual range in thermal solar installations and was fixed as constant with the aim of comparing the studied cases. Charge duration expressed as a dimensionless time t^*, was determined as follows:

$$t^* = (Q_{in}t)/V_t \quad (1)$$

where t is time (min) and V_t is the tank volume in L.

Table 1. Experimental trials conducted for validating the simulations.

	Inflow	Ambient temperature
Trial	Q_{in} (L min^{-1})	T_{amb} (K)
E1-H-exp	16	295.4
E1-L-exp	6	295.6
D1-H-exp	16	297.2
D1-L-exp	6	293.3

E: Elbow. D: Sintered Bronze Conical Diffuser.
H: High (inflow) L: Low (inflow)

2.2 Numerical method

Three-dimensional Unsteady Reynolds-Average Navier-Stokes (URANS) simulations were performed using the STAR-CCM+ commercial code Ver. 6.04.014 [47]. The model is based on the mass and momentum conservation equations and on a finite-volume method [48] for solving the incompressible Navier-Stokes equations. For the purpose of mass conservation, a standard pressure correction algorithm (SIMPLE) was used. Similarly to the study in [39], comparisons with the laminar flow model were obtained. In these comparisons, differences were found in the upper part of the tank where the turbulent model more accurately predicted the stratification process. Thus, the results eventually presented in this paper are those obtained with a turbulent closure. For the turbulent closure, a standard k- ε model with a two-layer approach was used, which offers the most mesh flexibility [47]. The standard two-layer k- ε model is based on the standard k- ε [49] but was later modified to use the two-layer approach for resolving the viscous sublayer. The two-layer approach [50] allows the k- ε model to be applied in the viscous sublayer [47]. The computational scheme solves the incompressible Navier-Stokes equations in integral form for continuity and momentum [47]:

$$\frac{d}{dt}\int_V \rho\, dV + \oint_A \rho\, v \cdot da = 0 \tag{2}$$

$$\frac{d}{dt}\int_V \rho\, v\, dV + \oint_A \rho\, v \wedge v \cdot da = -\oint_A p\, \mathrm{I} \cdot da + \oint_A [\mathrm{T}] \cdot da + \int_V f_g\, dV \tag{3}$$

where ρ is density (kg m^{-3}); v is velocity (m s^{-1}); p is pressure (Pa); [T] is the viscous stress tensor; a is the face area vector; V is cell volume (m^3); A is cell area (m^2); I is the identity matrix; and f_g (N) is, in this case, the body force vector representing buoyancy effects.

Regarding the boundary conditions, the inflow was set using a uniform velocity profile and, for the outflow, a convective condition was applied. The inlet temperature T_{in} was fixed to 325.7 K for all cases. For the tank walls, a hybrid approach (all y^+ wall treatment) was set for the near-wall modelling, which was the recommended wall treatment for the standard two-layer k- ε model. This approach applies a model for non-dimensional wall distance y^+ larger than 30 and resolves the boundary layer in the other cases. The initial temperature of the water domain T_o was set to 293 K for all cases. For the external wall of the tank an adiabatic condition was set-up. The mathematical forms and their implementation can be consulted at [47] and the values are summarized in table 2. Following various trials, a time step of 1 s was selected as a proper solution time. A first-order upwind convection scheme was chosen for URANS solution with an implicit solver.

Water density was calculated, according to temperature (290-343 K), in each grid point at every time step, as follows:

$$\rho = 753.35 + 1.9057T - 0.00365T^2 \quad (4)$$

where T is temperature in K.

Likewise, specific heat capacity c (J kg^{-1} K^{-1}) was calculated as follows:

$$c = 5182.1 - 6.4901T + 0.0105T^2 \quad (5)$$

Dynamic viscosity μ (Pa s) was calculated as follows:

$$\mu = 10^{-1} - 8.63\cdot10^{-4}T + 2.51\cdot10^{-6}T^2 - 2.4510^{-9}T^3 \quad (6)$$

Finally, thermal conductivity λ (W m^{-1} K^{-1}) was also calculated:

$$\lambda = -3.07\cdot10^{-1} + 4.71\cdot10^{-3}T - 5.47\cdot10^{-6}T^2 \quad (7)$$

A second-order segregated fluid temperature model was employed. The segregated fluid temperature model solves the total energy equation with temperature as the independent variable, as follows:

$$\frac{d}{dt}\int_V \rho E\, dV + \oint_A [\rho H v]\cdot da = -\oint_A q''\cdot da + \oint_A [\mathrm{T}]\cdot v\, da + \int_V f\cdot v\, dV \quad (8)$$

where E is the total energy (J); H is the total enthalpy (J); q'' is the heat flux vector.

Regarding the mesh, in the water body, different structured grids were developed and tested to get an independent grid of 1,506,840 cells. This selection was based on a sensitivity analysis, which took into account comparison between simulations and experiments, convergence criteria and simulation time. In this work, the Grid Convergence Index (*GCI*), as calculated in [51], was used to estimate the convergence error. The *GCI* was obtained at several time steps using the different grids. The maximum *GCI* was

0.01% between the selected grid and the finer one. The geometrical variation between cells was kept to a value around 4%.

Since the objective of this work was to create a detailed simulation not only of the hydrodynamics, but also the heat transport in the tank, a structured grid was defined for both steel and fibreglass domains. The same procedure was used to select an independent grid for steel and fibreglass. Finally, the solid domains were made up of 92,154 grid points for steel and 275,487 grid points for fibreglass. The variation between cells was also kept to a value around 4%. The physical characteristics defined for the steel vessel were c_{st} = 477 J kg^{-1} K^{-1}, λ_{st} = 14.9 W m^{-1} K^{-1} and ρ_{st} = 7,900 kg m^{-3}. The physical characteristics defined for the fibreglass were c_{fg} = 835 J kg^{-1} K^{-1}, λ_{fg} = 0.043 W m^{-1} K^{-1} and ρ_{fg} = 16 kg m^{-3}. Some selected grid details are shown in Figure 2.

In all simulations energy transport was taken into account on the contact surfaces between the water, steel and fibreglass, which was performed with a contact interface. The contact interface condition is used in STAR-CCM+ [47] to join together two regions to permit heat transfer between them.

In order to diminish the complexity of the simulations and the computation time needed, some simplifications were made:

- The energy transport or losses produced in the material of diffusers or pipes were neglected.
- Although the ambient temperature in the experimental trials was between 293.3 K and 297.2 K, energy losses from the fibreglass to the surroundings were also neglected, considering the convective heat transfer coefficient in this border as equal to zero. This consideration was made by modelling the thermal specification of the boundary condition between fibreglass and the surrounding air as adiabatic.
- A slip wall boundary condition was used for the water domain.
- The water tank used in the experimental setup has two sets of thermocouples distributed uniformly. The geometry and place occupied by these probes where not considered.
- A manhole for visual inspection inside the storage was also omitted and a perfect cylinder wall was used instead.

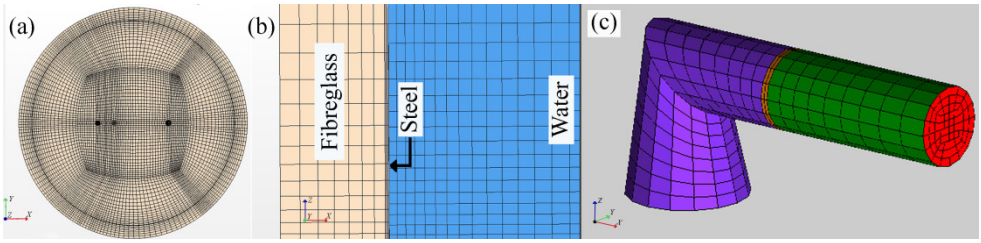

Fig. 2. Views of the mesh of the computational tank. (a) Top view of the tank. (b) Detail of the contact surfaces throughout the various materials. (c) View of the outlet elbow.

The validation of the CFD simulations was performed by comparing the evolution of the water temperature at each thermocouple position inside the tank determined experimentally and estimated from the CFD model.

Error rates were determined from each central and lateral thermocouple (TC and TL). Thus, the Mean Squared Error *MSE* (K^2) was calculated for each thermocouple to introduce a variance and bias of the error as follows:

$$MSE = \frac{1}{n}\sum_{i=1}^{n}\left(\hat{T}_i - T_i\right)^2 \quad (9)$$

where $\hat{T}_i$ (K) and T_i (K) are the experimental and computed values of temperature at each i^{th} experimental time step, and n is the number of experimental observations. Likewise, the Root Mean Squared Error *RMSE* (K) was calculated to estimate an error in the same units as the quantity being computed (temperature in K):

$$RMSE = \left(\frac{1}{n}\sum_{i=1}^{n}\left(\hat{T}_i - T_i\right)^2\right)^{0.5} \quad (10)$$

Finally, the Relative Error *RE* (%) was also calculated for each thermocouple at each experimental time step as follows:

$$RE = \left|\frac{T_i - \hat{T}_i}{\hat{T}_i}\right| 100 \quad (11)$$

2.3 Effect on the stratification of different inlet parameters

The experimental cases E1-H-exp, E1-L-exp, D1-H-exp and D1-L-exp described in [45], [46] and showed in Table 1 were used to validate the model. After validation, three additional configurations based on both geometrical variations of the elbow (E1) and the diffuser (D1), and modifications of the boundary condition or inlet velocity profile were simulated and analysed. Changes were implemented in order to study its influence on stratification. Details of the mesh in the various inlets of the computational tank are depicted in the Figure 3. Table 2 shows the inlet parameters for the different simulated cases. The different inlet configurations that were proposed (named E2, E3 and D2) are described below.

- E2: an elbow based on E1 geometry in which jet direction was horizontal, but in this case the velocity was modelled as a homogeneous profile in the nozzle tip section at the entrance of the water tank (Figure 3c). This profile could be managed with a flow stabilizer component, which in this case can be fitted before the nozzle tip of the inlet elbow, and can be used to smooth out turbulence. It should be

mentioned that the elbow internal domain was modelled for the E1 configuration (Figure 3a) in order to take into account the influence of the elbow geometry on the inlet velocity profile.

- E3: an elbow configuration with an upward course, with a homogeneous profile in the nozzle tip section (Figure 3d). The purpose of the E3 modelling case was to simulate an inlet similar to those commonly used in commercial hot water storage tanks.
- D2: a configuration in which the inflow goes through the lateral walls of the diffuser (Figure 3b). This proposal entailed a modification of the inlet boundary condition where the inflow could not go through the vertical direction of the diffuser. The proposal was about trying to find out if it was possible to improve stratification by blocking vertical velocity in the diffuser while an inflow was kept constant.

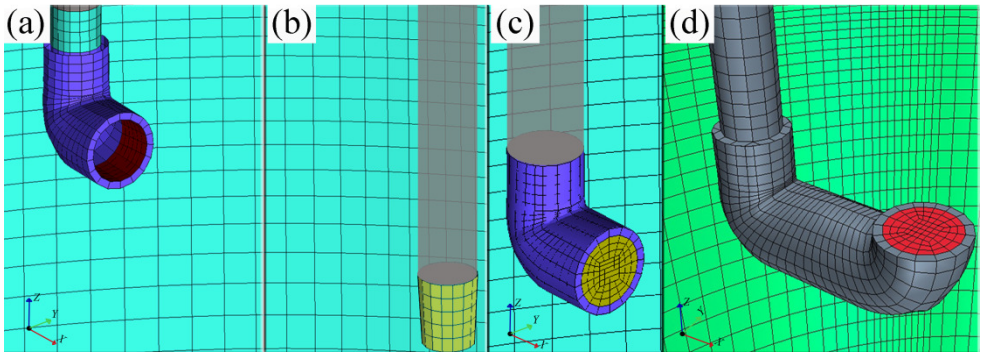

Fig. 3. Details of the mesh in the entrances of the computational tank. (a) View of the E1 inlet elbow. (b) View of the D1 inlet diffuser (the mesh used for D1 was the same as for D2). (c) View of the E2 inlet elbow. (d) View of the E3 inlet elbow.

In order to determine the effect of these inlet devices and two inflow rates (high H and low L), a comparative study of how temperature evolved with height was carried out. Simulations were carried out at a constant flow rate with a constant inlet temperature in order to be able to compare stratification between the studied cases.

The influence of the jet momentum flux M ($m^4\ s^{-2}$) in the inlet section of the tank was also analysed:

$$M = Q_{in}(m^3\ s^{-1})\ U_{jet}(m\ s^{-1}) \quad (12)$$

where jet velocity U_{jet} ($m\ s^{-1}$) is the area-weighted averaged velocity on the jet nozzle section entering the tank. Since Q_{in} and U_{jet} were modelled as constants, the M was also constant for each simulation case. A residence time t_r (min) was calculated as follows:

$$t_r = V_t/Q_{in} \quad (13)$$

Thus, each case was simulated for a specific charge time t_{ct} (min), which was calculated as the 120% of the residence time t_r.

Table 2. Inlet device and hydraulic inlet parameters for all simulated cases.

Simulated case	Jet direction	Jet velocity profile (**)	Inflow	Charge Time	Jet velocity	Jet momentum flux
			Q_{in} (L min^{-1})	t_{ct} (min)	U_{jet} (m s^{-1})	M (m^4 s^{-2})
E1-H (*)	horizontal	simulated	16	67.9	5.3 10^{-1}	1.41 10^{-4}
E1-L (*)	horizontal	simulated	6	180.9	2.0 10^{-1}	1.99 10^{-5}
E2-H	horizontal	homogeneous	16	67.9	5.3 10^{-1}	1.41 10^{-4}
E2-L	horizontal	homogeneous	6	180.9	2.0 10^{-1}	1.99 10^{-5}
E3-H	upwards	homogeneous	16	67.9	5.3 10^{-1}	1.41 10^{-4}
E3-L	upwards	homogeneous	6	180.9	2.0 10^{-1}	1.99 10^{-5}
D1-H (*)	horizontal & downwards	homogeneous	16	67.9	1.1 10^{-1}	2.99 10^{-5}
D1-L (*)	horizontal & downwards	homogeneous	6	180.9	4.2 10^{-2}	4.20 10^{-6}
D2-H	horizontal	homogeneous	16	67.9	1.3 10^{-1}	3.50 10^{-5}
D2-L	horizontal	homogeneous	6	180.9	4.9 10^{-2}	4.92 10^{-6}

(*): Simulations used to validate the CFD model.
(**): Simulated means that inlet internal domain was modelled; homogeneous means constant profile perpendicular to the inlet section.
Initial water temperature T_o (which coincided with the steel and fibreglass initial temperature) was in all cases 293 K. Inlet temperature T_{in} was always 325.7 K.

Different analyses and procedures were considered and discussed in order to study the influence of the tested inlet devices and inflows. Velocity contours along with water streamtraces and their relation to stratification, as well as temperature contours in water and through tank walls were represented and analysed at different times. The procedures which were used in this work are listed below.

2.3.1 Temperature profiles

The graphic representations of the instantaneous temperature profiles were analysed to compare stratification in the various simulation cases. Thermocline was determined and compared for each simulated case.

According to [26], thermocline thickness was defined in relation to a dimensionless temperature θ, with $\theta = (T - T_{in})/(T_o - T_{in})$.

In this work, thermocline thickness was estimated at a given instant as the distance between the two temperature profile points for which $\theta = 0.14$ and $\theta = 0.86$, respectively.

2.3.2 Thermal charging efficiency

Chan *et al.* [5] defined thermal storage efficiency for charging and discharging η. This efficiency, based on the first law of thermodynamics, was applied to a TES with initial uniform temperature during a charge or discharge period. In order to calculate η, mass flow must be fixed and the inlet temperature must be constant and different from the initial temperature:

$$\eta = \frac{\rho c V_t [T_{avg} - T_o]}{\rho c Q_{in} t [T_{in} - T_o]} = \frac{[T_{avg} - T_o]}{[T_{in} - T_o] t^*} \quad (14)$$

where T_{avg} is the volume-weighted average temperature in the water domain at each time step. This index calculates the effective energy stored estimating the relation between the energy change and the energy change that would have been produced in the same case for an ideal plug-flow at time t. This formulation considers ρ and c constants.

In the simulations performed in the present work, ρ and c were not considered as constant, but as depending on T in each grid point at every time step. Therefore, charge efficiency was calculated in two different ways in order to check the influence of these parameters in such efficiency: ρ and c as constants and, on the other hand, ρ and c as functions of T. Thus, the expression to calculate the efficiency proposed in [5] was used in this study but taking into account the variability of ρ and c according to T in each grid point at every time step. The expression used here was defined as:

$$\eta = \frac{V_t \left[\int_{T_o}^{T_{avg}} \rho c dT \right]}{Q_{in} t \left[\int_{T_o}^{T_{in}} \rho c dT \right]} = \frac{\int_{T_o}^{T_{avg}} \rho c dT}{\left[\int_{T_o}^{T_{in}} \rho c dT \right] t^*} \quad (15)$$

3 Results and discussion

3.1 Validation of the numerical results

Figure 4 depicts a comparison during the charge period between experimental and simulated temperatures (normalized with T_{in}), as a function of the dimensionless time (defined in eq. 1), in the thermocouple locations. For sake of brevity, only central thermocouples are shown.

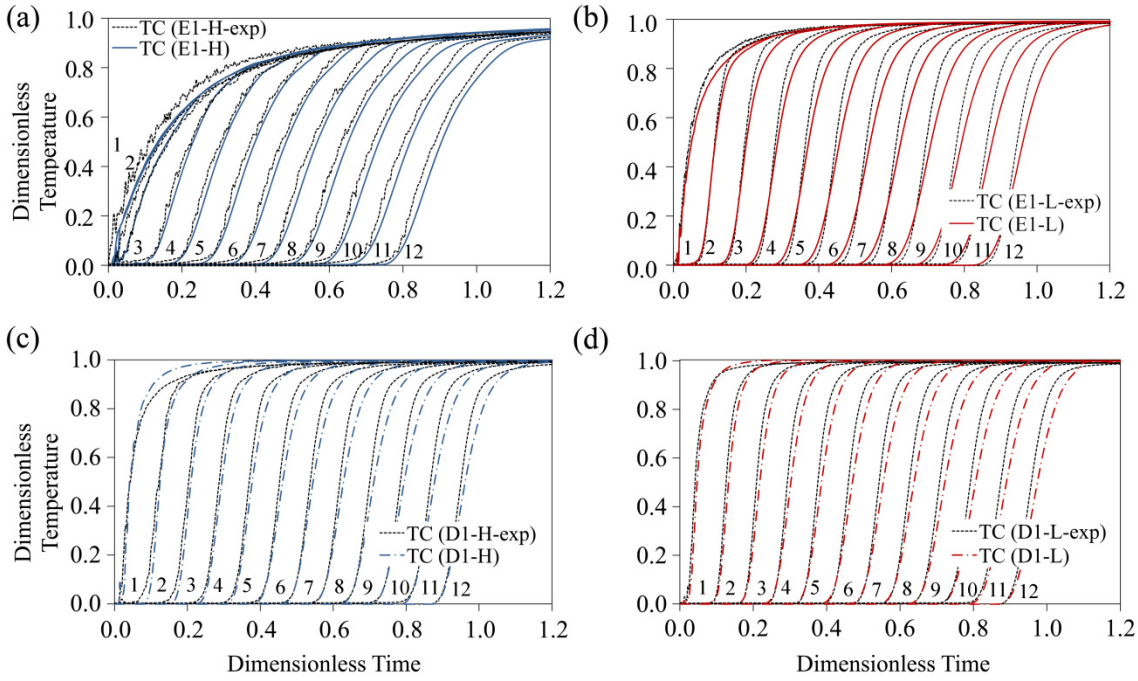

Fig. 4. Validation of the numerical results. Evolution of the water temperature in the central zone TC depending on dimensionless time t^*, determined experimentally and estimated from the CFD model. (a) E1-H case (b) E1-L case (c) D1-H and (d) D1-L case. Temperature was normalized with T_{in}.

A good correlation was found between the numerical and the experimental results in all cases, both in the central and in the lateral thermocouple positions (data not shown). The increase of temperature started almost at the same time and with a similar trend in both the experiments and simulations. Moreover, the evolution of the temperature of the experimental and simulated curves had a very similar slope and shape until the maximum temperature was reached. Table 3 presents the range of error rates of the validation cases for the 24 thermocouples during the charge time. The maximum *MSE* was 1.94 K^2 at the bottom part of the tank, near the outlet elbow (values registered by TL12) in the D1-L simulation. Likewise, the maximum *RMSE* was 1.39 K, near a lateral-top position (TL2) in the D1-L simulation. Finally, the maximum *RE* was 2.38%, in the lateral-top of the tank (TL1) of the D1-H simulation, at 100 s from the beginning of the charge (when 2.95% of the V_t was replaced). Larger errors were always found at the first stages of the charging process for all validation cases. These maximum errors could have been produced because of the beginning of the simulation process, which simulated a jet flow entering into an initially homogeneous fluid in the tank and can result in instability and mayor inaccuracies in the first stages of the calculus.

Simulated curves described smooth trend in all cases. Nevertheless, as was shown in [45], temperature shows clear disturbance in E1-H-exp trial. This was more severe for the central stratum of the top of the tank (TC1). However, it may be noted that few fluctuations were found in the high stratum of the other experimental trials. This effect was higher when inflow rate was larger and indicates the degree of mixing

in the tank due to the hot water inflow [45]. The URANS technique computes variable flow and temperature. This variable flow is a time averaged solution at each time step and seems less able to accurately describe the process for high inflow rates in this case.

Table 3. Range of error rates of the validation cases for the 24 thermocouples into the water tank**.**

	MSE (K^2)	*RMSE* (K)	*RE* (%)
E1-H	[0.1570 - 1.3658]	[0.3962 - 1.1687]	[0.44 - 2.03]
E1-L	[0.1158 - 1.5972]	[0.3403 - 1.2638]	[0.56 - 1.57]
D1-H	[0.4425 - 1.2742]	[0.6652 - 1.1288]	[1.01 - 2.38]
D1-L	[0.3986 - 1.9441]	[0.6313 - 1.3943]	[1.11 - 1.79]

Temperature at each thermocouple location rose almost at the same time in the experiments and simulations. Nevertheless, a time lag was observed between computed and experimental temperatures. These results indicate a different degree of mixing in the model compared to experiments which could be explained because the energy losses from valves and connecting pipes, as well as energy losses from the fibreglass to the surroundings were neglected.

Nevertheless, in spite of small discrepancies, the model satisfactorily reproduced the water temperature profile at both central and lateral zones. Therefore, the model proved to be reliable when applied to different inlet devices within the range of inflow rates tested in this study.

3.2 Sensitivity analysis of inlet parameters

This section presents a comparison among the results of the five configurations studied and the two inflows tested (Table 2).

3.2.1 Hydrodynamics and stratification

Numerical velocity results are presented and compared in this section. Only high inflow cases (16 L min^{-1}) are shown, since this analysis gave similar flow pattern results for the low inflow cases.

Figure 5 represents normal U_n (m s^{-1}) and tangential U_t (m s^{-1}) velocity in *XZ*-central profile on the section plane of the nozzle tip of upper elbow for simulations E1-H, E2-H and E3-H (Table 2). The evolution of the flow inside the elbow of the E1-H case caused a wedge-shaped profile in the inlet with U_n near a maximum of 1 m s^{-1} and a minimum of almost -0.3 m s^{-1}. On the other hand, E2-H and E3-H cases had a homogeneous velocity profile in their nozzle tip sections (Table 2). According to U_t, the E1-H case produced a sinuous profile with a maximum of 0.038 m s^{-1} and a minimum of -0.04 m s^{-1}. In contrast, U_t in E2-H and E3-H was equal to zero, since the velocity in these cases was defined as a boundary condition with velocity normal to the inlet plane.

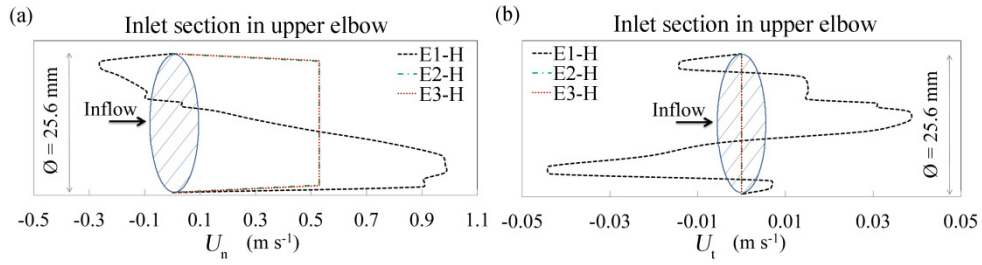

Fig. 5. Normal (a) and tangential (b) velocity in *XZ*-profile on the section plane of the nozzle tip of upper elbow (inflow) for simulations E1-H, E2-H and E3-H.

These differences in the inlet velocity profile might influence the velocity field in the upper part of the tank and subsequently, the stratification process. Furthermore, in order to properly model the inlet velocity profile in the nozzle tip for the E1 configuration, which was essential to manage good accordance with experimental results, it was important to note the relevance of accurately defining the inner-elbow grid and the geometrical boundary conditions. These aspects seem to suggest a significant influence of the inlet geometry on the stratification process in this case.

Figure 6 shows contours of the velocity vector module *U* and streamlines of flow in a middle vertical section in the tank near the inlets for the high inflow simulated cases (E1-H, E2-H, E3-H, D1-H and D2-H) at t = 17 min (fully developed flow). In all cases, the inflow formed large-scale recirculating structures which could be observed from X = 0.2 m to X = 0.4 m at different heights, depending on the case. It is also possible to identify a relatively small recirculation cell inside the elbow in the case E1 for both flows tested, which must cause the wedge-shaped profile in its nozzle tip. On the other hand, the jet flowed uniformly towards the opposite wall when the inflow entered the tank homogenously from the E2 configuration. In this case, the water flowed horizontally in the upper part of the tank and the large scale recirculating structure was located in a lower position (near Z = 1.45 m, level not shown in the Figure 6). Conversely, in the case of inflow through E3, the jet disturbed upwards, towards the top wall of the tank, and generated a large-scale recirculating structure closer to the upper part (Z = 1.66 m), reducing velocity considerably. Furthermore, for the D1-H case, the inlet velocity was modelled with a homogeneous value (Table 2), towards the lateral and downwards. The large scale recirculating structure was formed in the highest part of the tank (Z = 1.71 m). Finally, velocity was modelled with a homogeneous value (Table 2) for D2-H, flowing horizontally. In the case of the latter, the large scale recirculating structure was located further down (Z = 1.65 m).

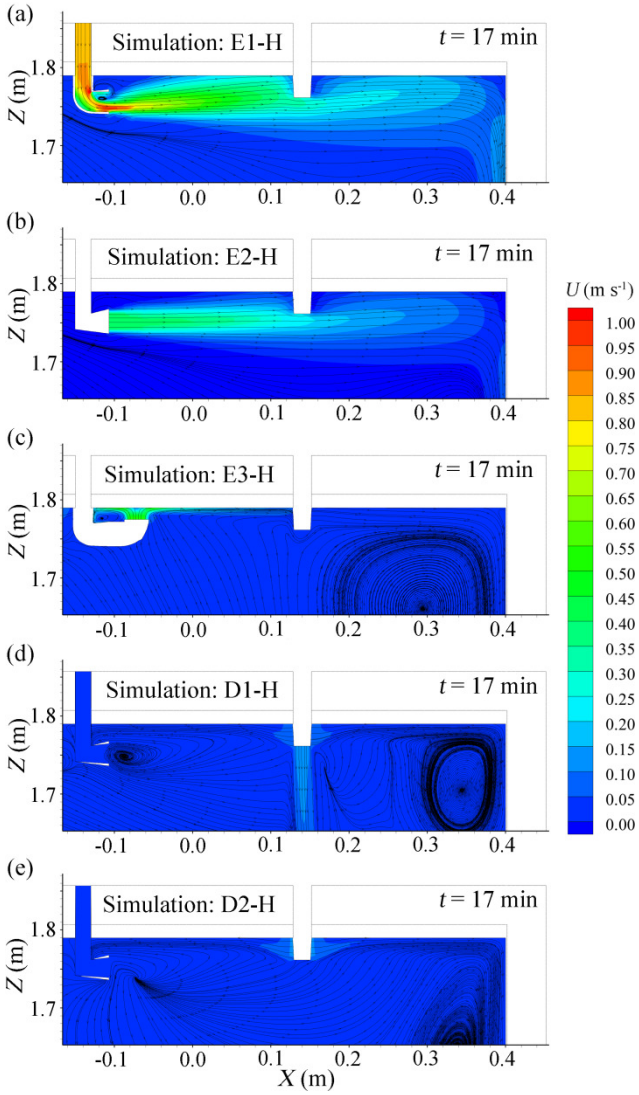

Fig. 6. Contours of the velocity vector module U and streamlines of flow in a middle vertical section near the inlets for the high inflow simulated cases (E1-H, E2-H, E3-H, D1-H and D1-H) at t = 17 min.

The volume-weighted average velocity magnitude $\overline{U}$ (m s^{-1}) in the water tank was also calculated in order to compare the different configurations. $\overline{U}$ was equal to $8.8 \cdot 10^{-3}$ m s^{-1} for E1-H, $7.1 \cdot 10^{-3}$ m s^{-1} for E2-H, $5.3 \cdot 10^{-3}$ m s^{-1} for E3-H, $1.6 \cdot 10^{-3}$ m s^{-1} for D1-H and $2.3 \cdot 10^{-3}$ m s^{-1} for D1-H. Thus, small variations of inflow characteristics as well as the geometrical inlet modifications can induce changes in the velocity field in terms of magnitude, which might induce changes in the stratification process.

Moreover, as illustrated in Figure 6, the aforementioned small recirculation cell inside the elbow (E1) produced the wedge-shaped profile observed, which implies a reduced effective area for the inflow entering the tank through the nozzle tip and, as a consequence, higher inlet velocity values. Furthermore, the fluctuations in the temperature due to turbulence commented by [45] might be created by such small recirculation, the effects of which were largely influenced by the inflow. The wedge-shaped profile,

together with the fluctuations due to turbulence induced by E1, may be one important mechanism producing mixing in these cases.

3.2.2 Temperature distribution

In this section, details of the distribution of temperature contours were compared. Although there were differences between D1 and D2 configurations in terms of jet velocity and jet momentum flux (Table 2), as well as flow pattern (Fig. 6), significant temperature differences between the two configurations were not found. Due to the absence of such differences, the more detailed analysis of water temperature contours will only be shown for D1-H and D1-L cases in order to simplify the display and comparison of the pictures (Fig. 7).

Figure 7 gives an accurate picture of temperature distribution with high inflow (top panels) for cases E1-H, E2-H, E3-H and D1-H at $t^* = 0.6$ ($t = 33.9$ min). The differences originated by inlet configurations in the stratification process are identified in detail, as well as the distribution of the temperature through the steel and fibreglass domains. It is possible to see how the temperature gradient between the hottest and the coldest water was the least stratified, both in width and in the lower position of the front in the E1-H case, followed by E2-H and E3-H. At this time, stratification was reasonably developed in E1-H and E2-H cases, although the influence of the jet on the original elbow configuration (E1) is clearly noticeable in the upper part of the tank due to the mixing caused by the small recirculation into the elbow. Stratification differences between E1-H and E2-H were only the result of the change of the velocity profile in the nozzle tip of the elbow (Fig. 5 and Fig. 6). Thus, smoothing out the velocity inlet (E2) seemed to appreciably reduce the degree of mixing in the upper part and the progress of the temperature front. Furthermore, when high inflow was operated upwards in a vertical direction near the top of the tank (Fig. 6c) through a hypothetical elbow (E3), the stratification level was considerably increased. This modification of the inflow direction induced changes in advection and, as a consequence, a reduction of almost 40% in the volume-weighted average velocity magnitude $\overline{U}$, from $8.8 \cdot 10^{-3}$ m s^{-1} to $5.3 \cdot 10^{-3}$ m s^{-1}, which seemed to significantly improve stratification for the elbow. On the other hand, stratification was better when inflow took place through the diffusers and the large-scale recirculating structure (Fig. 6d,e) kept closer to the upper part of the tank. It is also especially important to mention the similarities in the stratification level found between E3-H case and diffusers as the charge progressed, besides the differences in U_{jet} and M among E3-H, D1-H and D2-H, showed in Table 2. According to these results, regardless of the improvements made with the elbow, the best-stratified layers were obtained by the diffusers when high inflow was operated. This snapshot also shows how temperature was distributed

through the solid materials of the tank and the differences between each simulated case. Temperature in the walls was higher as the temperature front advanced more slowly, as was expected (*i.e.* D1-H and D2-H). Moreover, a low temperature distribution throughout the top fibreglass wall was kept during charge, due to the wall thickness of the steel (the thickness of the lateral wall of steel was 1.9 mm, while the bottom and top walls of steel were 17.2 mm).

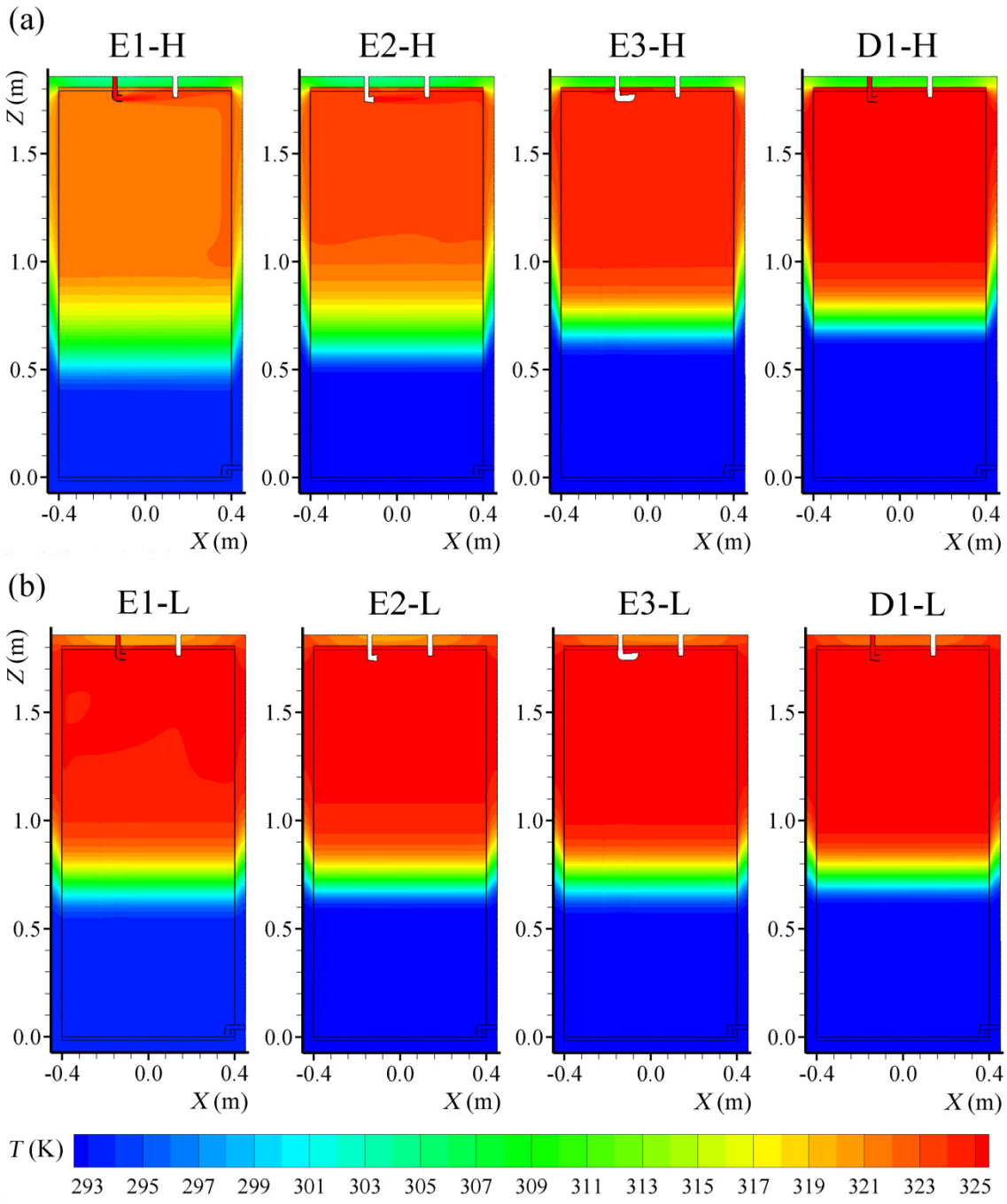

Fig. 7. Details of the distribution of temperatures for four of the simulated inlet devices at $t^* = 0.6$ (60% of V_t replaced). Temperature contours are presented in the symmetrical *XZ*-plane. (a) high inflow (E1-H, E2-H, E3-H and D1-H). (b) low inflow (E1-L, E2-L, E3-L and D1-L).

When low inflow was simulated, the evolution of the water layers was more similar between the tested configurations. This fact is shown in Fig. 7 (bottom panels), which illustrates for E1-L, E2-L, E3-L and D1-L temperature evolution at $t^* = 0.6$ ($t = 90.5$ min). In contrast to high inflow at this dimensionless filling time, stratification was apparently developed for all elbow cases and the thicknesses of their water layers were thinner at this stage, indicating a greater level of stratification. E1-L was the case which seemed to show a lower degree of stratification in terms of temperature gradient (lower position and more width), which indicates a higher level of mixing. Although the differences were small, the diffusers gave the best stratification during charge for low inflow (higher position and less width of the temperature gradient). Temperatures throughout the solid materials were distributed similarly for all simulated inlets when inflow was reduced, although higher temperatures were reached with the diffusers, due to their higher level of water stratification and the slowness of the temperature front. With this low inflow, temperature distribution throughout the top fibreglass wall was higher than for the high inflow, due to the longer time required for charging the same volume of water.

A comparison of the evolution of the dimensionless water temperature, depending on dimensionless time, in the TC (TC1, TC5, TC8 and TC12) during the charge period of the three inlet elbows for the simulated high and low inflow (Table 2) is depicted in Figure 8 (left panels). With the exception of the early stages of the first positions (TC1 and TL1) in E1-H, no significant differences were found between lateral stratum into the tank (TL) and the central one (TC). This effect was largely due to the aforementioned small recirculation in E1-H at the beginning of the charge and was reduced over time. Therefore, the analysis of temperature evolution will only be shown for TC. Regarding the high inflow (Fig. 8a), the temperature rose more quickly when the velocity inlet was smoothed out (E2-H) and even more when inflow operated upwards in a vertical direction near the top of the tank (E3-H), as the different slope of the curves indicates. Except for the first positions (TC1), in E2-H the temperature front reached lower locations later than E1-H and even later for E3-H, which represents an improvement in the stratification performance. Moreover, the smaller temperature slope of the curve in the upper part of the tank (TC1) indicated the high level of mixing introduced by the original elbow with high inflow (E1-H). In contrast, higher slopes were observed in this thermocouple for E2-H and E3-H, which indicates that mixing can be considerably reduced in this part of the tank. Consequently, the influence of higher inflow on stratification was reduced with the new elbow proposals. In addition, as was studied experimentally by [45], in the case of the elbow E1, the temperature did not reach the value of the inlet temperature, representing mixing in upper layers, even by the end of the charging and however the inflow tested. On

the other hand, the maximum temperature reached by the thermocouples of the E2-H simulation was higher than the original (E1-H) and became higher when E3-H was simulated. However, they did not reach the maximum value (T_{in}=325.7 K). When low inflow was simulated (Fig. 8c), slight differences were found between the elbow configurations. For the three elbows, the slope of the curves increased when inflow was reduced and became similar in all of them. In such reduced inflow, the highest possible temperature (T_{in}) was almost reached by most of the thermocouples under the new configurations (E2-L and E3-L). The progress of the temperature front was slower in comparison to the high inflow cases, although the temperatures recorded in E1-L showed that the increase in temperature started slightly sooner in comparison with the new proposals. Furthermore, slight differences were found in the upper part of the water tank (TC1), where temperatures reached higher values for the new elbows and, then, experienced a reduction in the mixing produced by the inlet. In view of the above, the stratification level in the E1 case could improve significantly by substituting the E1 inlet elbow with the E2 elbow, and it could improve even more by installing the E3 elbow.

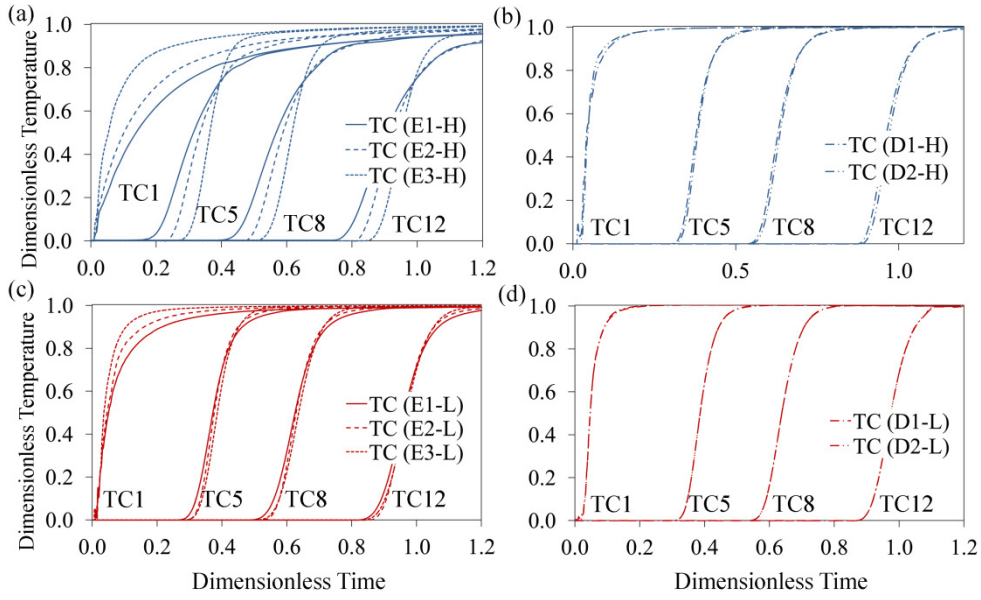

Fig. 8. Evolution of the dimensionless water temperature in the central zone TC depending on dimensionless time t^*. Top (high inflow): (a) simulations E1-H, E2-H and E3-H; (b) simulations D1-H and D2-H. Bottom (low inflow): (c) simulations E1-L, E2-L and E3-L; (d) simulations D1-L and D2-L.

Figure 8 (right panels) also compared the evolution of the dimensionless water temperature of the two inlet diffusers for the high and low inflow simulations (Table 2). The rest of the thermocouples, which are not plotted, showed a similar pattern. Regarding the simulated high inflow (Fig. 8b), the temperature front reached each thermocouple location practically at the same time between diffusers, with no significant differences. Compared to the elbow cases (Fig. 8a), the temperature front progressed more slowly when flow was through diffusers. Moreover, in these cases the temperature rose faster than in elbow

simulations. This numerical evidence demonstrates that a stratification performance with diffusers was better than one with the original elbow (E1), (as was already discussed by [45]) and also better than the new elbow proposals (E2 and E3), although no relevant differences were found between D1 and D2. Unlike in the elbow cases, during charge the maximum temperature reached by all thermocouples with diffuser cases was very close to T_{in}, which represents a high level of mixing. Likewise, for such diffusers, there were no clear differences when inflow was reduced to 6 L min^{-1} (Fig. 8d), except for the highest possible temperature (T_{in}), which seemed to be reached slightly better here than in the high inflow cases (Fig. 8b), particularly for the upper part of the water tank (TC2). This was already reported by [46] when D1-H-exp and D1-L-exp were compared. The beginning of the curves seemed to get closer in all the inlet configurations when low inflow (Fig. 8c and d) was compared, nevertheless, it was slower when flow was charged through diffusers. For all simulated configurations and inflows, the increase in temperature at each TC location started practically at the same time as each TL, suggesting a plug-flow type. However, Fig. 7a showed disrupted temperature layers at same heights in the hottest water stratum when the high flow was simulated through E1 and E2. Moreover, in such figures, it is possible to discern a small plume coming from the elbows (E1 and E2). In this way, and for these specific cases, the solely use of experimental data which provide only discrete measures might result in a vague procedure to represent temperature distribution and, consequently, properly characterize thermal stratification in water storage. Thus, it was possible to obtain further insights from the computed data.

According to these qualitative results, lower inflow reduced mixing for all simulated inlet configurations. Although there were less differences between all the elbows for low inflow, this evidence indicates a higher degree of stratification when the velocity inlet was smoothed out (E2-H and E2-L) and even more when inflow operated upwards (E3-H and E3-L). In the case E2, it was avoided the aforementioned small recirculation cell (seen in E1 case, Fig 6a), which cause the jet wedge-shaped profile and is associated with higher velocities and fluctuations due to turbulence. In the case E3, the improvement in stratification was due to the considerable reduction of velocity achieved because the jet impinged on the top wall. Thus, the influence on mixing by a higher flow in the original elbow case could be reduced by using the new proposed elbow configurations (E2 and E3). However, even though the inflow tested diffusers (D1and D2) were similar, they illustrated a better stratification performance than all the elbow simulations. In these cases, the inflow had a uniform velocity, towards the lateral and downwards, which reduces considerably the velocities into the tank. By blocking vertical velocity in the diffuser (D2) did not

lead to improve stratification in comparison with D1 due to the small area representing the vertical wall of the diffuser (7% of the total area) in relation to the lateral one.

3.2.3 Thermocline

The graphic representation of the instantaneous temperature vertical-profile in the central region was analysed to compare the degree of stratification between the various cases at several simulation times. Thermocline was determined from temperature profiles and compared between the simulated cases. In addition, the thermocline thickness and its middle point were also calculated. As with the temperature contours (Fig. 7) and due to the fact that there were no significant differences between diffusers in terms of their temperature profiles, the more detailed analysis of temperature profiles will only be shown for the D1-H and D1-L cases, in order to display and compare the cases more easily.

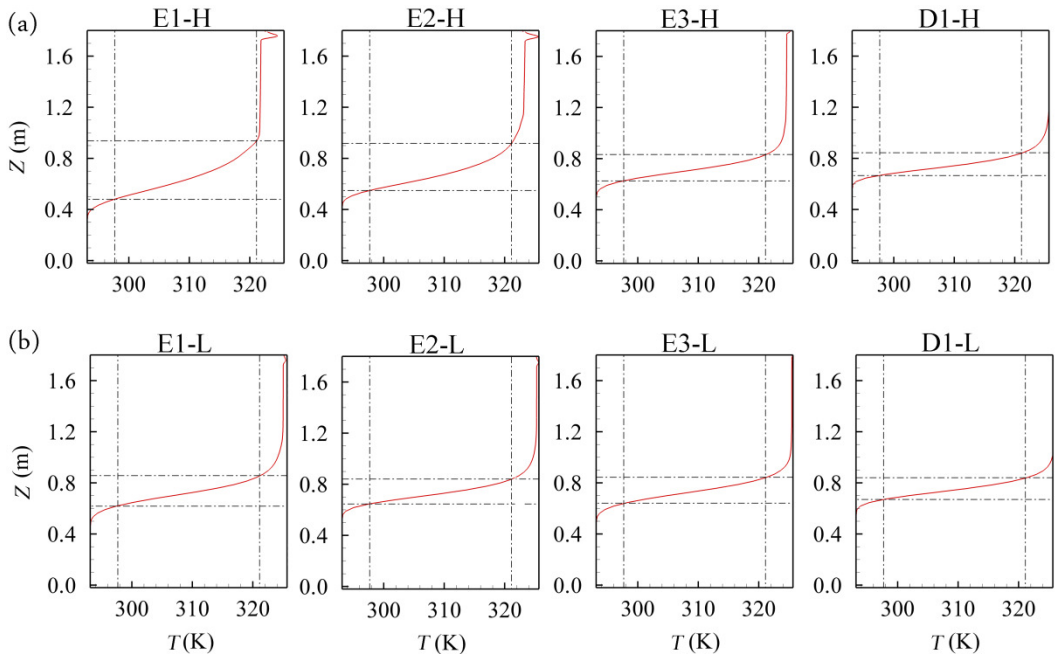

Fig. 9. Temperature profiles in the central region (TC probe) for four of the simulated inlet devices at $t^* = 0.6$ (60% of V_t replaced). (a) high inflow (E1-H, E2-H, E3-H and D1-H). (b) low inflow (E1-L, E2-L, E3-L and D1-L). Thermocline is estimated in each case with a θ between 0.14 and 0.86.

Figure 9a depicts temperature profiles for the simulated inlet devices with the high inflow at dimensionless filling time of 0.6 (t = 33.9 min). Thus, it is possible to appreciate graphically the thermocline thickness and its middle point and compare the cases. At this charging time, the numerical values of thermocline thickness were 46 cm, 37 cm, 20 cm and 17 cm for E1-H, E2-H, E3-H and D1-H respectively. The middle point was 71 cm, 73 cm, 73 cm and 75 cm for E1-H, E2-H, E3-H and D1-H respectively. In the E1-H case, the numerical temperature did not reach the inlet water temperature and showed a peak in its profile near the top of the tank, which was clearly induced by the simulated jet flow.

This indicates the aforementioned high degree of mixing at the top of the tank. This effect was also seen with E2-H, although somewhat less so in this case. In contrast, when inflow was operated through the elbow upwards (E3-H), no clear influence of jet flow was found and the maximum possible temperature was nearly reached, showing a stratification performance close to diffusers (D1-H and D2-H) with this high flow. This last modification of the elbow seemed to produce an effect similar to diffusers in terms of bulk velocity, direction and profile of the velocity inlet. As was suggested in previous sections and regarding the degree of stratification for high inflow, diffusers were the best stratified cases. The worst case was E1-H, followed by E2-H and E3-H. In these cases, the differences in stratification were mostly related to advection in the high stratums of the tank, which was largely induced by the inlet device geometry and direction (Fig. 5 and Fig. 6).

Figure 8b shows temperature vertical profiles for the simulated inlet devices with low inflow at dimensionless filling time of 0.6 (t = 90.5 min). At this time, the numerical values of thermocline thickness were 23 cm, 19 cm, 20 cm and 17 cm for E1-L, E2-L, E3-L and D1-L respectively. The middle point was 74 cm in all cases except in D1-L, in which it was 75 cm. There were fewer differences between inlet configurations when low inflow was simulated. Although the degree of stratification was considerably improved for elbow cases when inflow was lower, no significant differences were found for diffuser cases. Nevertheless, the best stratified cases for low inflow were again diffusers (D1-L and D2-L) and the worst case was E1-L.

Some experimental [10] and numerical [38] studies reported the destratifying effect produced by higher flows. In this way, the inflow level is seen as a parameter affecting the degree of stratification. In [43], different inlet diffuser designs of a solar hot water storage tank during charging with constant mass flow rate and inlet temperature were studied by CFD experiments. A recommendation for the maximum velocities or Reynolds numbers was to be found for the analyzed inlets and flow rates based on the displacement of the thermocline for the different hydraulic diameters and mass flow rate. In such study, the Reynolds number of the flow at the end of the entering pipe was found to be a good indicator for the disturbance of stratification. However, assessing the Reynolds number and comparing in the case of the porous wall of the diffuser in our study could be a no consistent task. On the other hand, as was pointed out by [45] and supplemented in this work, the inflow does not always appear to be effective enough in determining an expected level of mixing and, consequently, inducing a destratifying effect. This is proven in this research because diffusers with 16 L min^{-1} gave better stratification than all simulated elbows with 6 L min^{-1}. In addition, the hydraulic diameter or the cross-sectional inlet velocity (referred here as jet

velocity) do not even appear to be a good indicator of mixing. Moreover, for configurations in this study tested during thermal charging, jet momentum flux M and jet velocity U_{jet} did not actually seem appropriate as a parametric characteristic being related to stratification as equal M and U_{jet} for the three elbows (Table 2) gave significant differences in this transient process. In addition, M for the three elbows with low inflow was less than M for diffusers with high inflow, whereas stratification for D1-H and D2-H was better than for E1-L, E2-L and E3-L. On the other hand, mixing near inlets can significantly affect stratification in TES during charging and this could be induced by the inner geometrical configurations of such inlets and jet direction. In particular, it might be more important to take into account inlet velocity and its characteristics (Fig. 6 and 7), for instance in terms of direction and velocity profile in the inlet nozzle tip (U_n and U_t), when greater stratification performance is intended.

In these cases, with constant inflow and inlet temperature, thermocline thickness can be used as a good indicator of the stratification level. Moreover, the width of the thermocline may be related to stored energy degradation. However, this parameter cannot itself provide a quantitative energy degradation level [24], which is of interest for designers.

Finally, although the operating condition of E1-H is not usual in practice, it can be of interest in specific research. In fact, other thermocline techniques based on experimental data recorded only in vertical probe position, such as linear interpolation, could result in different vertical temperature profiles if they were to be tested in a lateral position into the tank (TL) instead of a central position (TC). In these cases, in which a three-dimensional flow into the tank is produced, instead of a plug-flow type, CFD procedures can supplement such techniques.

3.2.4 Thermal charging efficiency

In order to estimate the fraction of effective energy stored and compare the different configurations and inflows, thermal charging efficiency was calculated for each simulation. Thermal charging efficiency takes values ranging from zero to one, with one representing perfect efficiency for charging, while zero expresses a situation of total inefficiency. As already stated in Section 2.3.2, since ρ and c were not considered as constant in the CFD model implemented in this work, with a view to verify the influence of these parameters, charging efficiency was calculated in two different ways: with Eq. (14) (efficiency proposed in [5] which considers ρ and c as constant), and with Eq. (15) (efficiency based in [5] but taking into account the variability of ρ and c). It was found that the differences over time between the results obtained from Eqs. (14) and (15) were negligible in all cases, with the greatest discrepancy being 0.005 for E3-H. This means that, when this efficiency was applied in these cases, there was no relevance in

considering the ρ and c as depending on T. The results shown below are those which were computed with the ρ and c as constant values.

As with the other sections and due to the absence of significant differences in this thermal charging efficiency between diffuser configurations (D1 and D2), the more detailed analysis will only be shown for the D1-H and D1-L cases.

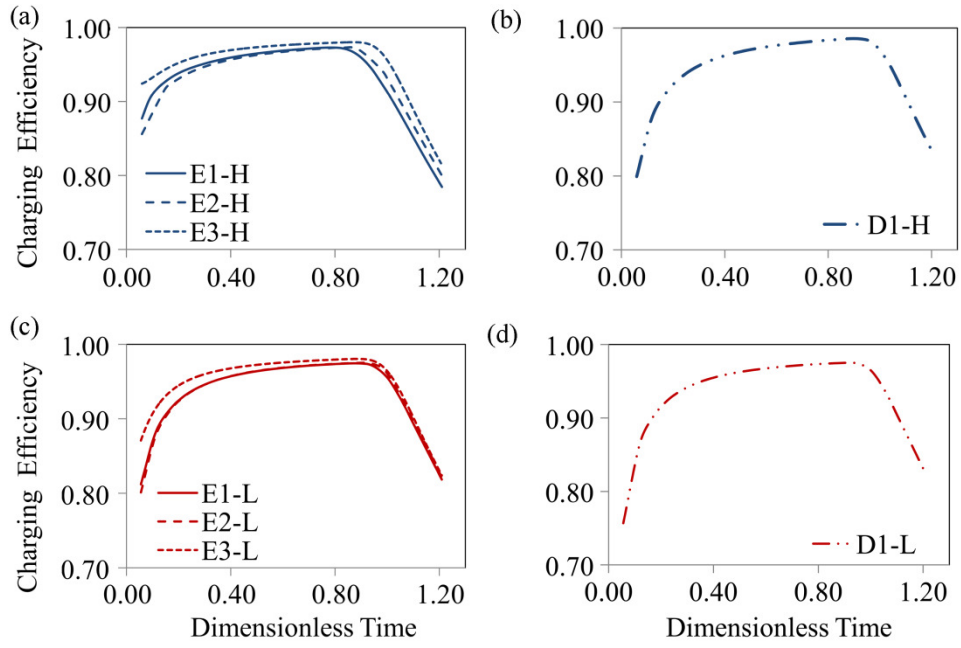

Fig. 10. Evolution of the thermal storage efficiency as proposed by [5] during the charge period (120% V_t replaced) depending on dimensionless time t^*. Top (high inflow): (a) simulations E1-H, E2-H and E3-H; (b) simulation D1-H. Bottom (low inflow): (c) simulations E1-L, E2-L and E3-L; (d) simulation D1-L.

A comparison of the evolution of thermal storage efficiency in simulations with high and low inflow during the charge period (which lasted until 120% of V_t was replaced), is shown in Figure 10. The thermal efficiency started with values equal to zero and rose during thermal charge to a maximum when the thermal charge was close to 100% of the V_t replaced, starting then to descend. This was due primarily to mixing at the beginning of the charge, induced by the incoming water, warmer than the water previously stored in the tank at $T = T_o$. A higher level of mixing can cause the hot water to start to flow through the outlet pipe before and thus negatively affect efficiency. Once the dimensionless time of 1.00 was reached (100% of the V_t injected), this efficiency fell rapidly as the T_{avg} could not increase as time progressed (Eq. 14).

Although no significant differences were found between all the cases, the best result, $\eta = 0.98$, was reached by the diffuser with high inflow at $t^* = 0.91$ (Fig. 10b). Energy losses through wall materials and diffusion between the hottest and the coldest water could induce considerable degradation of stratification if charging takes a long time and therefore can produce a reduction of the effective energy stored. Thus,

that might be the reason why higher values of charging efficiency were reached by the diffuser with the high inflow instead of the low inflow. Nevertheless, between t^* of 0.2 and 0.9, the storage efficiencies were above 0.90 for all cases, which was considered as a high efficiency for charging.

When elbows with high inflow were compared (Fig. 10a), E3-H achieved the best efficiency, reaching at $t^* = 0.86$ a value of $\eta = 0.97$. The greatest difference between E3-H and E2-H was almost 0.07 at the beginning of the charge (6% of V_t replaced). When the same comparison was made with low inflow (Fig. 10c), E1-L and E2-L showed very few differences between them, with E3-L achieving the best result, reaching at $t^* = 0.89$ a value of $\eta = 0.97$. In this inflow case, the greatest disparity was again about 0.07 at the beginning of the charge (6% of V_t replaced). These contrasts between elbows can be considered small in terms of effective energy stored.

When high inflow was simulated (Fig. 10a,b), charging efficiency with E3-H was higher than with diffuser until $t^* = 0.6$, after which efficiency with diffuser was higher. In contrast, the results were noteworthy when elbows and diffuser were compared for low inflow (Fig. 10c,d), with E3-L achieving a higher charging efficiency than diffuser when 100% of the V_t replaced, showing a maximum difference of 0.11 at the beginning of the charge.

Although, these efficiency results indicated better effective energy stored during charging for E3 and diffuser configurations, the differences were considered to be of little importance when all the simulated cases were compared. However, this parameter only evaluates the fraction of effective energy stored, but the quality of the energy charged would need further analysis to be correctly understood. Finally, it is also worth mentioning that the rest of the analysis and parameters studied in this work confirm that diffusers favour water stratification during thermal charging of the tank at constant temperature with both low and high flows.

4 Conclusions

In this work, the results of three-dimensional URANS simulations were presented for a hot water storage tank with constant inflow and inlet temperature during a thermal charge process. CFD techniques were used to numerically study hydrodynamics and temperature over time in the water domain and wall materials. In the simulations the distribution of the temperature could be determined throughout the computational domain while in the experiment only a few points could be measured. Therefore, it was possible to obtain further insights from the computed data. Moreover, the model was implemented for studying the influence of some inlet configurations on stratification and then improving thermal

performance in the tank. This methodology can be used to improve the design and optimization of the solar energy systems used in buildings.

The model was implemented and validated with experimental measurements for two inflows and two different inlet devices (elbow and diffuser) with a high degree of correlation between experimental and computed temperatures. After validation, three new inlet configuration based on simple modification of original ones were analysed in order to study its influence on stratification. By this, it was intended more specifically to provide easy-to-implement and low-cost inlet modifications in the tank.

When the velocity in the nozzle tip section of the elbow was modelled defining a homogeneous profile during high inflow charge (E2-H), the inlet velocity values were lower than for the original elbow (E1-H), reducing the mixing in the upper part of the tank. In the case of the same inlet was operated upwards (E3-H), the velocity magnitude in the tank was considerably reduced, which implied a further reduction of mixing and then, a better stratification level. Moreover, when the low inflow (6 L min^{-1}) was simulated, less mixing differences were found between the three elbows modelled (E1-L, E2-L and E3-L), although the hot front progressed more slowly than with high inflow and the highest possible temperature in the tank (T_{in}) was almost reached by most of the thermocouples. On the other hand, when the inflow was modelled as a horizontal inlet for the diffuser (D2-H), no significant effect was observed with regards to original diffuser (D1-H); for diffusers with low inflow (D1-L and D2-L), there were few discrepancies in comparison with high inflow and no evident differences between them, representing the best temperature distribution among all the simulations.

In this research, the degree of stratification seemed to be mostly affected by inlet direction and inlet velocity profile, which is produced by inlet designs. In this way, the high influence of the flow in the case of the original elbow (E1) could be technically reduced using these proposals (E2 and E3). Nonetheless, the degree of stratification in the simulated cases suggested the convenience of using a sintered bronze conical diffuser as an inlet, instead of elbows, since it not only gave better results, but also practically constant behaviour for the tested inflow range.

Finally, the thermal efficiency at each time step was calculated for each simulation case during charging to estimate the fraction of effective energy stored. Although, this efficiency indicated better effective energy stored during charging for E3 and both diffuser configurations, minor differences were found between them.

5 Acknowledgments

This research was supported by the Plan Nacional de I+D+i del Ministerio de Ciencia e Innovación (ENE2009-13376). The authors would like to thank L.H. Sanchis for his valuable and constructive suggestions during the planning and development of this research.

6 References

[1] Y. M. Han, R. Z. Wang, and Y. J. Dai, 'Thermal stratification within the water tank', *Renew. Sustain. Energy Rev.*, vol. 13, no. 5, pp. 1014–1026, Jun. 2009.

[2] R. Shukla, K. Sumathy, P. Erickson, and J. Gong, 'Recent advances in the solar water heating systems: A review', *Renew. Sustain. Energy Rev.*, vol. 19, pp. 173–190, Mar. 2013.

[3] I. Dinçer and M. Rosen, *Thermal Energy Storage: Systems and Applications*, İbrahim Dinçer, Marc A. Rosen. New York, USA: John Wiley & Sons, 2002.

[4] C. A. Cruickshank and S. J. Harrison, 'Heat loss characteristics for a typical solar domestic hot water storage', *Energy Build.*, vol. 42, no. 10, pp. 1703–1710, Oct. 2010.

[5] A. M. C. Chan, P. S. Smereka, and D. Giusti, 'A Numerical Study of Transient Mixed Convection Flows in a Thermal Storage Tank', *J. Sol. Energy Eng.*, vol. 105, no. 3, pp. 246–253, Agosto 1983.

[6] J. Van Berkel, 'Mixing in thermally stratified energy stores', *Sol. Energy*, vol. 58, no. 4, pp. 203–211, Oct. 1996.

[7] T. Giglio and R. Lamberts, 'Savings related to solar water heating system: A case study of low-income families in Brazil', *Energy Build.*, vol. 130, pp. 434–442, Oct. 2016.

[8] C. Cristofari, G. Notton, P. Poggi, and A. Louche, 'Influence of the flow rate and the tank stratification degree on the performances of a solar flat-plate collector', *Int. J. Therm. Sci.*, vol. 42, no. 5, pp. 455–469, May 2003.

[9] U. Jordan and S. Furbo, 'Thermal stratification in small solar domestic storage tanks caused by draw-offs', *Sol. Energy*, vol. 78, no. 2, pp. 291–300, Feb. 2005.

[10] A. A. Hegazy, 'Effect of inlet design on the performance of storage-type domestic electrical water heaters', *Appl. Energy*, vol. 84, no. 12, pp. 1338–1355, Dec. 2007.

[11] L. J. Shah and S. Furbo, 'Entrance effects in solar storage tanks', *Sol. Energy*, vol. 75, no. 4, pp. 337–348, Oct. 2003.

[12] M.-S. Shin, H.-S. Kim, D.-S. Jang, S.-N. Lee, Y.-S. Lee, and H.-G. Yoon, 'Numerical and experimental study on the design of a stratified thermal storage system', *Appl. Therm. Eng.*, vol. 24, no. 1, pp. 17–27, Enero 2004.

[13] E. Andersen, S. Furbo, and J. Fan, 'Multilayer fabric stratification pipes for solar tanks', *Sol. Energy*, vol. 81, no. 10, pp. 1219–1226, Oct. 2007.

[14] A. Aviv, Y. Blyakhman, O. Beeri, G. Ziskind, and R. Letan, 'Experimental and Numerical Study of Mixing in a Hot-Water Storage Tank', *J. Sol. Energy Eng.*, vol. 131, no. 1, pp. 011011–011011, Enero 2009.

[15] J. D. Chung, S. H. Cho, C. S. Tae, and H. Yoo, 'The effect of diffuser configuration on thermal stratification in a rectangular storage tank', *Renew. Energy*, vol. 33, no. 10, pp. 2236–2245, Oct. 2008.

[16] E. Hahne and Y. Chen, 'Numerical study of flow and heat transfer characteristics in hot water stores', *Sol. Energy*, vol. 64, no. 1–3, pp. 9–18, Sep. 1998.

[17] P. Steinert, S. Göppert, and B. Platzer, 'Transient calculation of charge and discharge cycles in thermally stratified energy storages', *Sol. Energy*, vol. 97, pp. 505–516, Nov. 2013.

[18] J. van Berkel, C. C. M. Rindt, and A. A. van Steenhoven, 'Thermocline dynamics in a thermally stratified store', *Int. J. Heat Mass Transf.*, vol. 45, no. 2, pp. 343–356, Enero 2002.

[19] Y. H. Zurigat, P. R. Liche, and A. J. Ghajar, 'Influence of inlet geometry on mixing in thermocline thermal energy storage', *Int. J. Heat Mass Transf.*, vol. 34, no. 1, pp. 115–125, Enero 1991.

[20] A. Castell, M. Medrano, C. Solé, and L. F. Cabeza, 'Dimensionless numbers used to characterize stratification in water tanks for discharging at low flow rates', *Renew. Energy*, vol. 35, no. 10, pp. 2192–2199, Oct. 2010.

[21] M. Y. Haller, C. A. Cruickshank, W. Streicher, S. J. Harrison, E. Andersen, and S. Furbo, 'Methods to determine stratification efficiency of thermal energy storage processes – Review and theoretical comparison', *Sol. Energy*, vol. 83, no. 10, pp. 1847–1860, Oct. 2009.

[22] A. Mawire and S. H. Taole, 'A comparison of experimental thermal stratification parameters for an oil/pebble-bed thermal energy storage (TES) system during charging', *Appl. Energy*, vol. 88, no. 12, pp. 4766–4778, Diciembre 2011.

[23] V. Panthalookaran, W. Heidemann, and H. Mueller-Steinhagen, 'A new method of characterization for stratified thermal energy stores', *Sol. Energy*, vol. 81, no. 8, pp. 1043–1054, 2007.

[24] Y. H. Zurigat and A. J. Ghajar, 'Heat transfer and stratification in sensible heat storage systems', in *Thermal Energy Storage. Systems and Applications*, New York, USA: John Wiley & Sons, 2002, pp. 259–301.

[25] W. P. Bahnfleth and J. Song, ‘Constant flow rate charging characteristics of a full-scale stratified chilled water storage tank with double-ring slotted pipe diffusers’, *Appl. Therm. Eng.*, vol. 25, no. 17–18, pp. 3067–3082, Diciembre 2005.

[26] A. Musser and W. P. Bahnfleth, ‘Evolution of temperature distribution in a full-scale stratified chilled-water storage tank with radial diffusers’, *ASHRAE Trans.*, vol. 104, Part 1, pp. 55–67, 1998.

[27] J. Yoo, M. W. Wildin, and C. R. Truman, ‘Initial formation of a thermocline in stratified thermal storage tanks’, presented at the ASHRAE Transactions, 1986, vol. 92, pp. 280–292.

[28] L. J. Shah, G. L. Morrison, and M. Behnia, ‘Characteristics Of Vertical Mantle Heat Exchangers For Solar Water Heaters’, *Sol. Energy*, vol. 67, no. 1–3, pp. 79–91, Jul. 1999.

[29] L. J. Shah and S. Furbo, ‘Correlation of experimental and theoretical heat transfer in mantle tanks used in low flow SDHW systems’, *Sol. Energy*, vol. 64, no. 4–6, pp. 245–256, Diciembre 1998.

[30] R. De Césaro Oliveski, A. Krenzinger, and H. A. Vielmo, ‘Comparison between models for the simulation of hot water storage tanks’, *Sol. Energy*, vol. 75, no. 2, pp. 121–134, Agosto 2003.

[31] K. Johannes, G. Fraisse, G. Achard, and G. Rusaouën, ‘Comparison of solar water tank storage modelling solutions’, *Sol. Energy*, vol. 79, no. 2, pp. 216–218, Agosto 2005.

[32] P. Armstrong, D. Ager, I. Thompson, and M. McCulloch, ‘Improving the energy storage capability of hot water tanks through wall material specification’, *Energy*, vol. 78, pp. 128–140, Diciembre 2014.

[33] A. J. Ghajar and Y. H. Zurigat, ‘Numerical Study of the Effect of Inlet Geometry on Stratification in Thermal Energy Storage’, *Numer. Heat Transf. Part Appl.*, vol. 19, no. 1, pp. 65–83, Enero 1991.

[34] N. Gopalakrishnan and S. S. Murthy, ‘Mixed convective flow and thermal stratification in hot water storage tanks during discharging mode’, *Appl. Sol. Energy*, vol. 45, no. 4, pp. 254–261, Mar. 2010.

[35] A. Musser and W. P. Bahnfleth, ‘Parametric Study of Charging Inlet Diffuser Performance in Stratified Chilled Water Storage Tanks with Radial Diffusers: Part 2–Dimensional Analysis, Parametric Simulations and Simplified Model Development’, *HVACR Res.*, vol. 7, no. 2, pp. 205–222, Abril 2001.

[36] S. Ievers and W. Lin, ‘Numerical simulation of three-dimensional flow dynamics in a hot water storage tank’, *Appl. Energy*, vol. 86, no. 12, pp. 2604–2614, Diciembre 2009.

[37] R. E. Spall, ‘A numerical study of transient mixed convection in cylindrical thermal storage tanks’, *Int. J. Heat Mass Transf.*, vol. 41, no. 13, pp. 2003–2011, Jul. 1998.

[38] W. Yaïci, M. Ghorab, E. Entchev, and S. Hayden, ‘Three-dimensional unsteady CFD simulations of a thermal storage tank performance for optimum design’, *Appl. Therm. Eng.*, vol. 60, no. 1–2, pp. 152–163, Oct. 2013.

[39] M. Gasque, P. González-Altozano, D. Maurer, I. J. Moncho-Esteve, R. P. Gutiérrez-Colomer, G. Palau-Salvador, E. García-Marí., ‘Study of the influence of inner lining material on thermal stratification in a hot water storage tank’, *Appl. Therm. Eng.*, vol. 75, pp. 344–356, Enero 2015.

[40] L. Kong, WeixingYuan, and N. Zhu, ‘CFD Simulations of Thermal Stratification Heat Storage Water Tank with an Inside Cylinder with Openings’, *Procedia Eng.*, vol. 146, pp. 394–399, 2016.

[41] R. Cònsul, I. Rodríguez, C. D. Pérez-Segarra, and M. Soria, ‘Virtual prototyping of storage tanks by means of three-dimensional CFD and heat transfer numerical simulations’, *Sol. Energy*, vol. 77, no. 2, pp. 179–191, 2004.

[42] L. J. Shah, E. Andersen, and S. Furbo, ‘Theoretical and experimental investigations of inlet stratifiers for solar storage tanks’, *Appl. Therm. Eng.*, vol. 25, no. 14–15, pp. 2086–2099, Oct. 2005.

[43] C. Gwerder, L. Lötscher, M. Kaufmann, A. Huggenberger, S. Boller, B. Meier, I. Mojic, M. I. Haller, ‘Horizontal Inlets of Water Storage Tanks With Low Disturbance of Stratification’, *J. Sol. Energy Eng.*, vol. 138, no. 5, pp. 051011–051011, Agosto 2016.

[44] S. Li, Y. Zhang, Y. Li, and X. Zhang, ‘Experimental study of inlet structure on the discharging performance of a solar water storage tank’, *Energy Build.*, vol. 70, pp. 490–496, Feb. 2014.

[45] E. García-Marí, M. Gasque, R. P. Gutiérrez-Colomer, F. Ibáñez, and P. González-Altozano, ‘A new inlet device that enhances thermal stratification during charging in a hot water storage tank’, *Appl. Therm. Eng.*, vol. 61, no. 2, pp. 663–669, Nov. 2013.

[46] P. González-Altozano, M. Gasque, F. Ibáñez, and R. P. Gutiérrez-Colomer, ‘New methodology for the characterisation of thermal performance in a hot water storage tank during charging’, *Appl. Therm. Eng.*, vol. 84, pp. 196–205, Jun. 2015.

[47] CD-Adapco, *Star-CCM+ User Guide*. Melville, NY, USA., 2011.

[48] H. K. Versteeg and W. Malalasekera, *An Introduction to Computational Fluid Dynamics: The Finite Volume Method*. New York, USA: Longman Scientific and Technical, 1998.

[49] W. P. Jones and B. E. Launder, 'The prediction of laminarization with a two-equation model of turbulence', *Int. J. Heat Mass Transf.*, vol. 15, no. 2, pp. 301–314, Feb. 1972.

[50] W. Rodi, 'Experience with two-layer models combining the k-epsilon model with a one-equation model near the wall', in *29th Aerospace Sciences Meeting. AIAA 91-0216*, Reno, NV, 1991.

[51] I. B. Celik, U. Ghia, P. J. Roache, C. J. Freitas, H. Coleman, and P. E. Raad, 'Procedure for Estimation and Reporting of Uncertainty Due to Discretization in CFD Applications', *J. Fluids Eng.*, vol. 130, no. 7, pp. 078001–078001, Jul. 2008.